Influence of Process Parameters on Microstructure and Mechanical Properties of Friction-Stir-Processed Mg-Gd-Y-Zr Casting

Q. YANG, B.L. XIAO, and Z.Y. MA

Mg-10Gd-3Y-0.5Zr (wt pct) casting was subjected to friction stir processing (FSP) at a constant rotation rate of 800 rpm and varied travel speeds of 25, 50, and 100 mm/minute. FSP resulted in the generation of fine-grained microstructure and fundamental dissolution of coarse $Mg_5(Gd,Y)$ phase at the grain boundaries, thereby enhancing the tensile properties significantly at both room and elevated temperatures. The grain size of the FSP samples decreased with the increasing travel speed, whereas the microstructure heterogeneity with the banded structure (onion rings) became evident at a higher travel speed. Tensile elongation of the FSP samples increased as the travel speed increased, whereas the highest strengths were obtained at the medium travel speed of 50 mm/minute. Higher strengths and greater elongations were observed for the FSP samples in the transverse direction (TD) than in the longitudinal direction (LD). After post-FSP aging, the strengths of the FSP samples were increased significantly with the TD and LD exhibiting the same strengths; however, the elongation was decreased remarkably with the TD having higher elongation than the LD. A variation of the tensile properties was discussed in detail based on the microstructure heterogeneity and fracture surfaces.

DOI: 10.1007/s11661-011-1076-2

I. INTRODUCTION

As the lightest metals, magnesium alloys have attracted increasing interest in recent years for potential applications in the aerospace, aircraft, and automotive industries.[1] However, the low strength and poor creep resistance at increased temperatures restrict their wide applications. Recently, Mg-RE alloys (RE represents rare earth elements) were developed to meet the demand for high temperature applications. The addition of RE elements can produce thermally stable second phases in the Mg matrix, leading to high strength at a high temperature as well as good creep resistance.[2]

Currently, the Mg-RE alloy parts are produced mainly by casting, and the microstructure of the castings is characterized by coarse grains and coarse eutectic networks at the grain boundaries. This microstructure limits the mechanical properties of the Mg-RE castings, especially the properties at a high temperature. Therefore, a modification of the microstructure is needed to enhance the mechanical properties and broaden the applications of Mg-RE alloys. Conventionally, heat treatment and various plastic deformation methods are applied to modify the microstructure of the Mg castings.[3,4] However, the heat treatment at high temperature for lengthy time not only is time consuming but also results in coarse grains. Furthermore, a lengthy heat treatment is also needed before plastic deformation occurs as a result of the poor formability of magnesium alloys.

Friction stir processing (FSP), which was developed based on the principle of friction stir welding (FSW), has been demonstrated to be an effective method for the microstructural modification of castings.[5,6] During FSP, a processed zone is obtained in just several minutes without preheating for the cast alloys. FSP of conventional cast magnesium alloys, such as AM60B, AZ80, and AZ91, resulted in significantly enhanced tensile and fatigue properties because of the grain refinement, the breakup and dissolution of second phase particles, and the elimination of porosity.[6–9]

The influences of FSP on the cast Mg-RE alloys were studied recently. Tsujikawa *et al.*[10] achieved the ultrafine grains and refined lamellar structure in cast Mg-5.5Y-4.3Zn by FSP; increased hardness was obtained. Freeney and Mishra[11] obtained a fine-grained microstructure with dispersed nanosized particles in EV31A casting by FSP, and the mechanical properties were improved significantly. Our previous study on cast Mg-Gd-Y-Zr indicated that FSP resulted in significant grain refinement and the dissolution of coarse eutectic $Mg_5(Gd,Y)$ phase, thereby enhancing the mechanical properties of Mg-Gd-Y-Zr alloy significantly.[12] However, the alternating fine- and coarse-grained bands were observed in the FSP Mg-Gd-Y-Zr alloy. These bands or onion rings were generally suggested to influence the mechanical properties of the FSW/FSP samples,[6,13,14] and they could be eliminated by adjusting the process parameter.[15] However, an investigation of the variation of the banded structure with the FSP parameter and its

Q. YANG, Postgraduate, and B.L. XIAO and Z.Y. MA, Professors, are with the Shenyang National Laboratory for Materials Science, Institute of Metal Research, Chinese Academy of Sciences, Shenyang 110016, P.R. China. Contact e-mail: zyma@imr.ac.cn
Manuscript submitted August 10, 2011.
Article published online February 10, 2012

influence on the mechanical properties of FSP Mg-Gd-Y-Zr alloy is lacking.

In this study, FSP at varied parameters was conducted on the cast Mg-Gd-Y-Zr with special attention being paid to the following: (1) the resultant microstructure, especially the banded structure under different FSP parameters; and (2) the tensile properties of various FSP samples in both the transverse and longitudinal directions at both room and high temperatures. The aim is to establish the relationship among the FSP parameter, banded structure, tensile properties, and fracture behavior.

II. EXPERIMENTAL

Mg-10Gd-3Y-0.5Zr (wt pct) ingot was used as the base metal (BM). Eight-millimeter-thick plates were machined from the as-received BM and then subjected to FSP at a constant rotation rate (ω) of 800 rpm and varied travel speeds (v) of 25, 50, and 100 mm/minute. A tool with a shoulder 20 mm in diameter and a threaded conical pin 8 mm in root diameter and 4.9 mm in length was used. After FSP, the aging treatment was conducted at 498 K (225 °C) for 13 h (hereafter referred to FSP-T5). For comparison, the BM was solution treated at 798 K (525 °C) for 10 h, quenched into cold water (referred to cast-T4), then aged at 498 K (225 °C) for 13 h (referred to cast-T6). The principle directions of the FSP samples were marked as the LD (longitudinal direction, along the FSP direction), the TD (transverse direction, transverse to the FSP direction), and the ND (normal direction, normal to the plate surface).

Microstructural observations were conducted by optical microscopy (OM), scanning electron microscopy (SEM; FEI Quanta 600; FEI Instruments,) equipped with energy-dispersive spectroscopy (EDS), and transmission electron microscopy (TEM, FEI Tecnai G^2 F20; FEI Company, Hillsboro, OR). The specimens for OM and SEM were cut in the TD-ND plane and prepared by mechanical polishing and etching using a solution of 6 g picric acid + 10 mL acetic acid + 70 mL ethanol + 10 mL water. The grain sizes were estimated by the linear intercept method. Electron backscatter diffraction (EBSD) orientation maps were obtained using a Zeiss Supra 35 (Carl Zeiss, Oberkochen, Germany), operated at 20 kV, and interfaced to an HKL Channel EBSD system (HKL Technology ApS, Hobro, Denmark). The specimens for EBSD were electropolished using a solution consisting of 60 mL nitric acid and 140 mL ethanol at 12 V and 243 K (−30 °C). Thin foils for TEM were prepared by low-energy ion milling.

Tensile specimens with a gage length of 2.5 mm and a gage width of 1.4 mm were machined from both the cast and FSP Mg-Gd-Y-Zr samples. The FSP specimens were machined along both the TD and LD with the gage being completely in the stir zone (SZ). For surface observation, the tensile specimens were mechanically polished and etched before the tensile test. The tensile tests were conducted at both room and high temperatures at a strain rate of 1×10^{-3} seconds^{-1}.

III. RESULTS

A. *Microstructure*

Figure 1 shows the optical macrographs of the transverse sections of the FSP samples at different travel speeds. All the SZs showed a nonsymmetric elliptical profile. The SZ under a travel speed of 25 mm/minute exhibited a relatively uniform structure. As the travel speed increased, the onion rings became obvious. At a high travel speed of 100 mm/minute, a void was found at the top of the SZ (Figure 1(c)).

Figure 2 shows the microstructures of the BM and region 1 (the center region of the SZ in Figure 1) in various FSP samples. The BM was characterized by coarse grains and eutectic $Mg_5(Gd,Y)$ networks at the grain boundaries (Figure 2(a)). The microstructures of the FSP samples were all composed of fine and equiaxed grains, and the average grain size decreased as the travel speed increased. For the travel speeds of 25, 50, and 100 mm/minute, the grain size was determined to be 8.4, 6.1, and 5.6 μm, respectively. Homogenous grains were observed in the SZ under a travel speed of 25 mm/minute, whereas the nonuniformity of grain size became evident as the travel speed increased (Figures 2(c) and (d)).

The OM microstructures of region 2 in the SZs are shown in Figure 3. The grains in these regions were equiaxed, and the average grain sizes were the same as in the centers of the SZs for all the FSP samples (Figure 2). Note that some narrow black bands approximately 1 to 5 μm in width aligned in discontinuous semicircles were distributed in these regions, which corresponded to the onion rings as shown in Figure 1. The width and continuity of these bands increased with increasing the travel speed. A careful observation revealed that these bands were composed mainly of fine grains ~2 μm in size.

The SEM images of region 1 in various FSP samples revealed the uniform microstructure without the remaining eutectic $Mg_5(Gd,Y)$ phase within the grains or at the grain boundaries (not shown); this finding was consistent with our previous study.[12] However, for the onion rings in region 2 of the SZs, besides the discontinuous fine-grained bands observed in Figure 3, the backscattered electron (BSE) images revealed the discontinuous white, gray and black bands alternated with each other in all the SZs, as shown in Figs. 4(a) through (c). These bands had a width of ~30 μm at a travel speed of 25 mm/minute, and the width increased as the travel speed increased. EDS analyses indicated that these bands had different solute contents. The grains in the white, gray and black bands had high solute contents (~14 wt pct Gd and ~4 wt pct Y), medium solute contents (~11 wt pct Gd and 3 wt pct Y), and low solute contents (~9 wt pct Gd and ~3 wt pct Y), respectively. In addition, as shown in Figure 4(d), a small amount of particle-rich bands with the particle size of approximately 1 μm were observed to be distributed along the white bands, and the number of particles increased as the travel speed increased. These particles were determined to be the $Mg_5(Gd,Y)$ phase by EDS. Such onion rings were also observed in the longitudinal section of

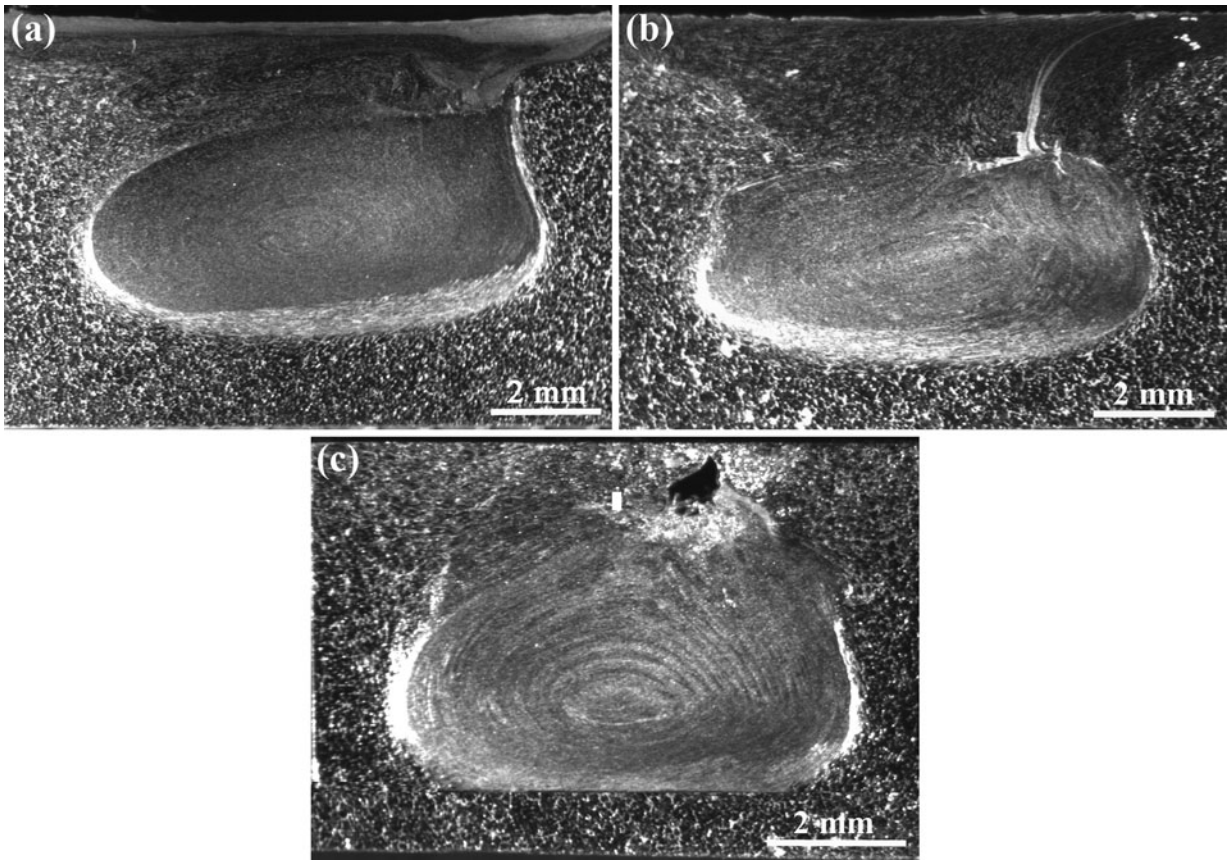

Fig. 1—Macrographs of transverse sections of FSP samples at 800 rpm and (*a*) 25 mm/min, (*b*) 50 mm/min, and (*c*) 100 mm/min (the advancing side is on the right).

the FSP samples; these discontinuous bands alternated with each other in a parallel of semicircular marks.

Figure 5 presents the TEM bright-field images of the cast-T6 and FSP-T5 (800 rpm, 25 mm/minute) samples. In both samples, a high density of fine plate-shaped precipitates (~50 nm in length) with three variants were distributed uniformly in the matrix with the incident electron beam approximately parallel to $[0001]_\alpha$. Selected-area electron diffraction (SAED) patterns indicated that these precipitates were the metastable β' phase and precipitated on the prismatic planes of the matrix. The size and density of these precipitates in both the cast-T6 and FSP-T5 samples were almost the same (Figures 5(a) and (b)). However, the precipitates at the grain boundaries were different. The discontinuous precipitates together with narrow precipitate-free zones (PFZs) were commonly observed in the cast-T6 sample but seldom detected in the FSP-T5 sample (Figures 5(c) and (d)).

B. *Tensile Properties*

The tensile properties of the cast-T4 and various FSP samples in the TD are shown in Table I.

Compared with the cast-T4 sample, the FSP samples exhibited significantly enhanced mechanical properties. The elongation of the FSP samples increased as the travel speed increased, whereas the strengths did not exhibit a continuous increase with the travel speed. For the FSP sample with the medium travel speed of 50 mm/minute, the highest ultimate tensile strength (UTS) of 363 MPa and yield strength (YS) of 281 MPa were achieved, whereas the sample with the highest travel speed of 100 mm/minute exhibited the lowest UTS and YS.

Figure 6 shows a comparison of the tensile fracture surfaces between the cast-T4 and FSP samples. The fractograph of the cast-T4 sample exhibited the predominant cleavage fracture with deep cleavage steps and small cleavage facets (Figure 6(a)). In contrast, the ductile fracture feature composed of equiaxed and fine dimples was observed for all the FSP samples (Figures 6(b) through (d)).

C. *Tensile Properties in the TD and LD*

Tensile tests in both the TD and LD were conducted for the FSP sample. To minimize the influence of grain size variation on the tensile properties, the FSP sample at 25 mm/minute with relatively uniform grain structure was selected. The tensile results for both the FSP and FSP-T5 samples are shown in Table II.

For the FSP sample, both the strengths and elongation were higher in the TD than in the LD. Large improvements in the UTS and YS were observed after post-FSP aging, but the elongation was reduced

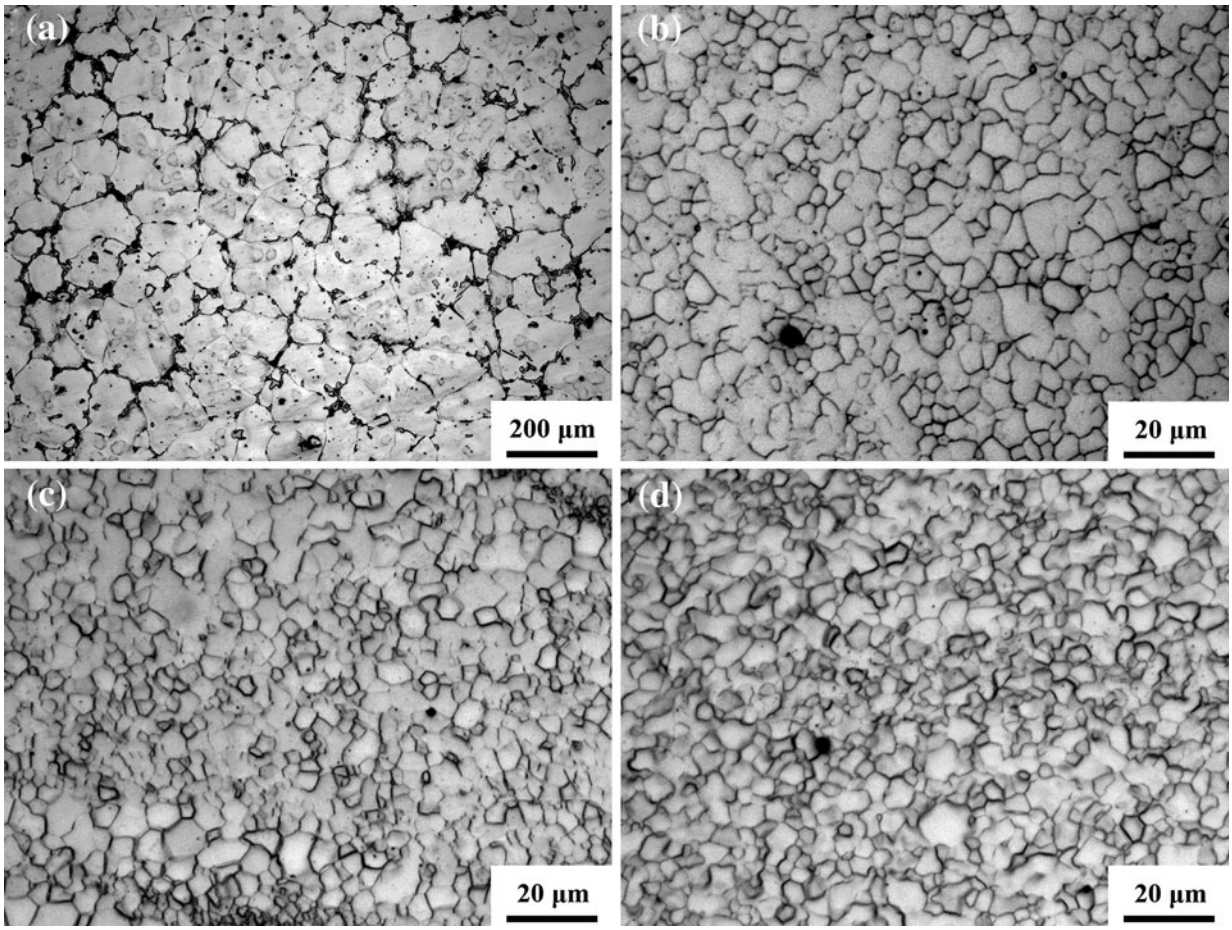

Fig. 2—Microstructure of (*a*) base metal and region 1 in the SZ as shown in Fig. 1 at different travel speeds: (*b*) 25 mm/min, (*c*) 50 mm/min, and (*d*) 100 mm/min.

remarkably. No distinct difference in the UTS and YS was observed for the FSP-T5 samples in the TD and LD, whereas a lower elongation was obtained in the LD.

BSE images of the longitudinal sections of the failed FSP and FSP-T5 samples are shown in Figure 7. For the TD specimen, the fracture path seemed to have no relation with the onion rings under both the FSP and FSP-T5 conditions (Figures 7(a) and (c)). However, for the LD specimen, the fracture path tended to follow the trace of the black bands in the FSP sample and was well along the white band in the FSP-T5 sample (Figures 7(b) and (d)). A magnified image of the fracture path as an insert in Figure 7(d) indicated that the white band was the narrow particle-rich band, where the particles were distributed mainly at the grain boundaries. Microvoids were found extensively in the interface between the grains and particles, and these microvoids were observed frequently in the particle bands near the fracture tip (Figure 7(e)).

The surfaces of the failed tensile specimens are shown in Figure 8. For the FSP sample in the TD tension, grain boundary sliding (GBS) or grain rotation with elongated grains was observed, extensive parallel slip lines and slip steps were distributed in the grains, and a small number of microcracks initiated mainly at the grain triple junctions (Figure 8(a)). However, for the LD specimen of the FSP sample, the slip lines were not observed extensively and the slip steps and GBS were not discernable, but a great number of cracks were distributed unevenly at the grain boundaries perpendicular to the tensile axis (Figure 8(b)). For the FSP-T5 sample, the surface of the failed TD specimen revealed the unevenly distributed straight and wavy slip lines in the grains, with some cracks being distributed at grain boundaries and along the slip lines, as indicated by the arrows in Figure 8(c). On the surface of the failed LD specimen, the slip lines were not observed distinctly, and besides the intergranular cracks, microvoids distributed at grain boundaries were detected frequently (Figure 8(d)).

The fracture surfaces of the FSP and FSP-T5 samples in the TD and LD are shown in Figure 9. For the FSP sample, as shown in Figure 9(a), the TD fracture surface showed a uniform ductile mode with the dimples distributed in the whole section of the fracture, as shown previously in Figure 6(b). On the LD fracture surface, besides the ductile fracture, part of region with a distinctly different fracture mode extended from the bottom to the middle section of the fracture surface, as marked by the dotted lines in Figure 9(b). A magnified view of this region revealed the brittle fracture feature of quasi-cleavage fracture and intergranular rupture, as

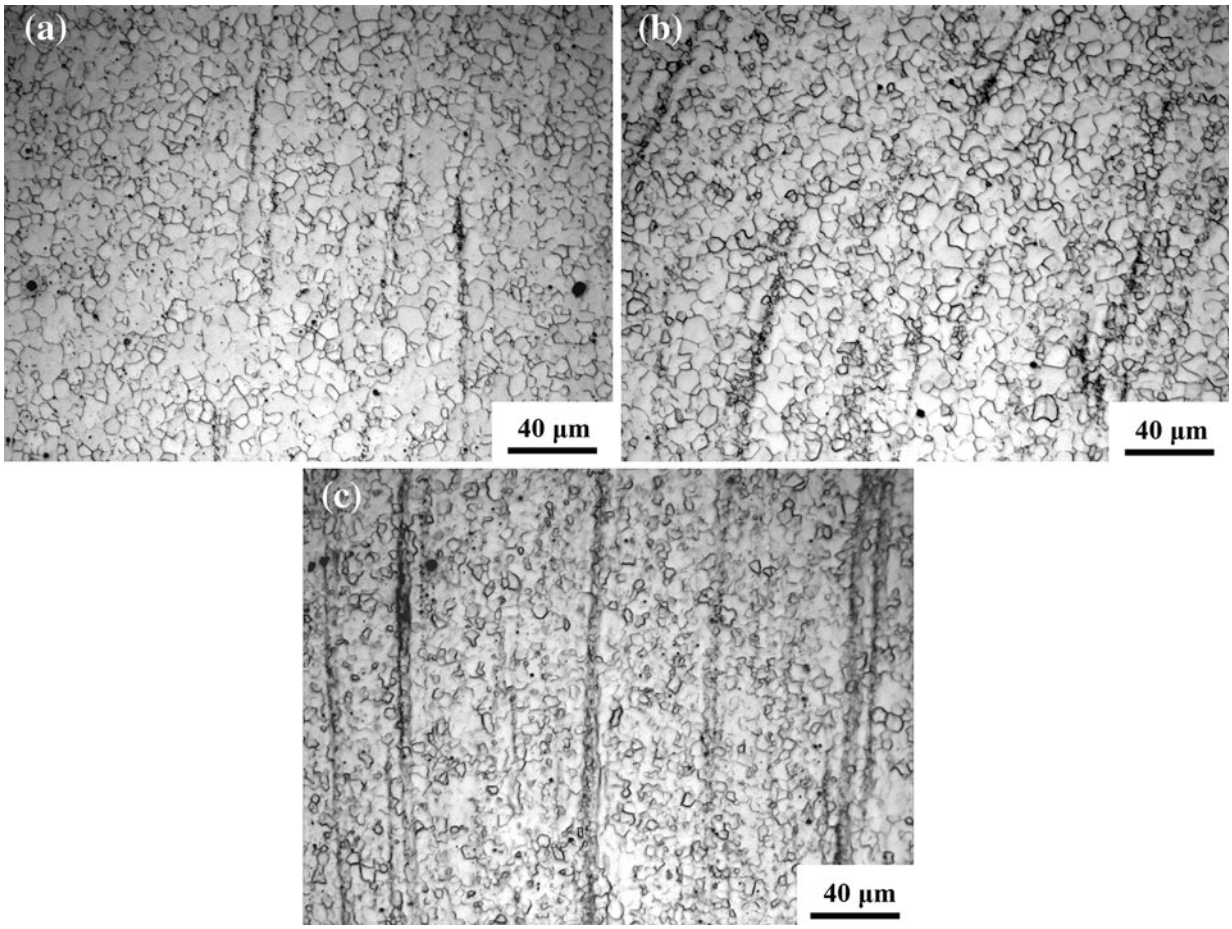

Fig. 3—Microstructure of region 2 in the SZ as shown in Fig. 1 at different travel speeds: (*a*) 25 mm/min, (*b*) 50 mm/min, and (*c*) 100 mm/min.

shown in Figure 9(e). For the FSP-T5 sample, a uniform fracture feature was observed in the TD specimen (Figure 9(c)), whereas in the LD specimen, a wide band of relatively different fracture surface was observed evidently in the middle section throughout the tensile specimen (Figure 9(d)); a magnified view of this region revealed small and flat dimples (Figure 9(f)).

D. *High-Temperature Tensile Properties*

The effects of temperature on the tensile properties of the aged Mg-Gd-Y-Zr samples are shown in Figure 10. It is noted that the cast-T6 sample showed a low strength of less than 250 MPa and the strength decreased almost monotonically from room temperature to 573 K (300 °C). By comparison, the FSP-T5 sample exhibited significantly enhanced strengths, and both the UTS and YS were almost unchanged from room temperature to 473 K (200 °C), but decreased quickly above 473 K (200 °C). In contrast, the elongation of both cast-T6 and FSP-T5 samples increased roughly with temperature, and the elongation of the FSP-T5 sample was higher than that of the cast-T6 sample at all temperatures.

Figure 11 shows the fracture morphologies of the cast-T6 specimens at various temperatures. The fractograph at room temperature exhibited brittle fracture composed of transgranular and intergranular rupture and deep cleavage steps, and some features on cleavage facets were observed (Figure 11(a)). As the temperature increased, the cleavage steps decreased, and the cleavage facets became smooth and featureless (Figures 11(c) and (e)). As observed from the longitudinal sections close to the fracture tip, twins were observed in all specimens, and their number decreased with increasing temperature (Figures 11(b), (d), and (f)). Cracks were observed only inside the grains, with some being associated with the deformation twins (as indicated by arrows). The number of the cracks along the twins increased with increasing temperature to 523 K (250 °C) but decreased at higher temperature of 573 K (300 °C) (Figures 11(b), (d), and (f)).

Figure 12 shows the fracture morphologies of the FSP-T5 sample at different temperatures. The fracture surfaces from room temperature to 523 K (250 °C) were almost the same and were characterized by the majority of quasi-cleavage fracture accompanied by a few intergranular cracks and small dimples (Figures 12(a) and (c)). The fracture surface at 573 K (300 °C) revealed the dominant intergranular rupture with fine dimples distributed densely in the fractured surfaces (Figure 12(e)). On the longitudinal sections close to the fracture tip,

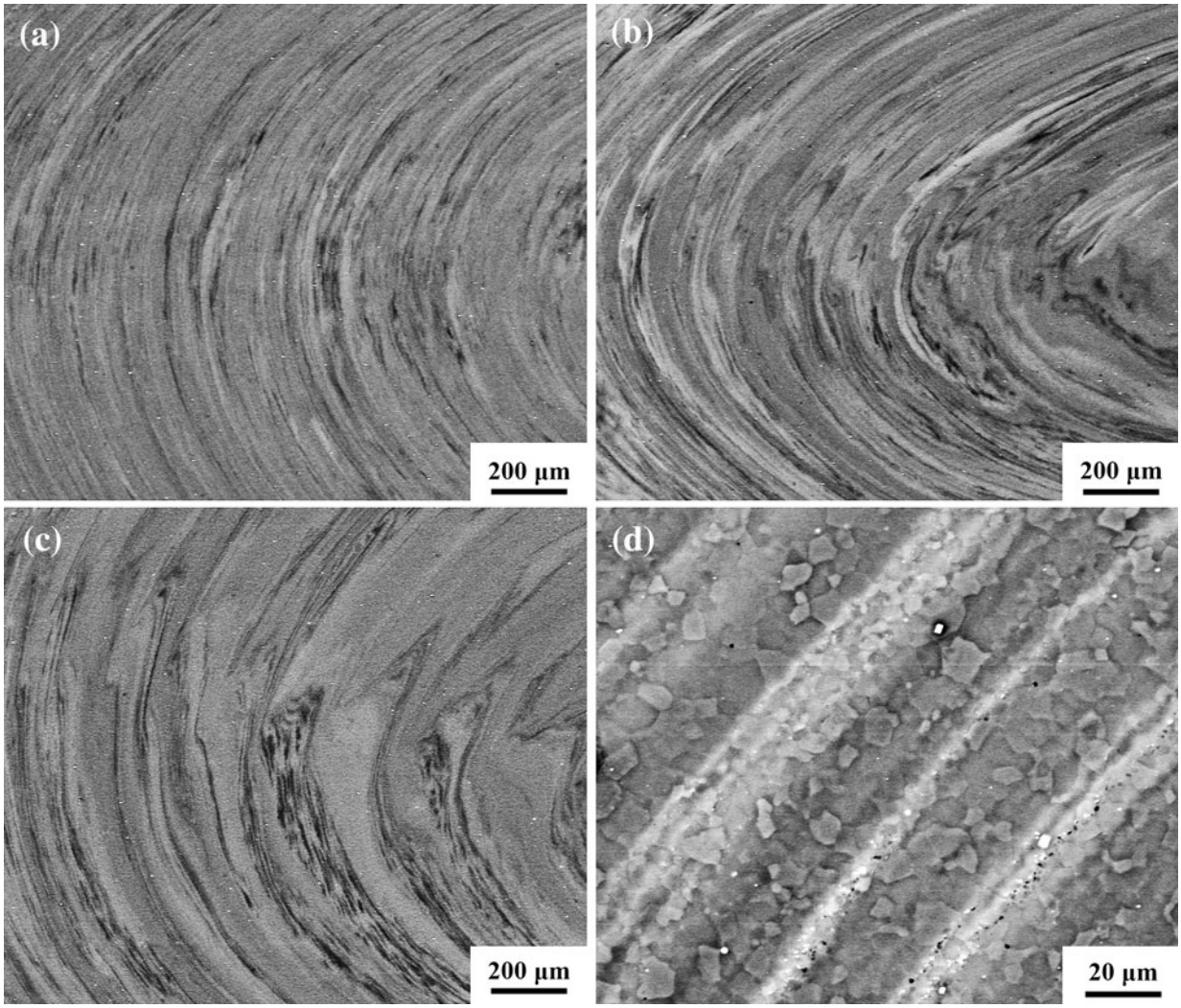

Fig. 4—SEM images of region 2 in the SZ as shown in Fig. 1 at different travel speeds: (*a*) 25 mm/min, (*b*) 50 mm/min, and (*c*) 100 mm/min. (*d*) A magnified image of the particle bands at 25 mm/min.

cavities were observed at the grain boundaries, and they tended to be elongated and interlinked perpendicular to the tensile direction as the temperature increased (Figures 12(b), (d), and (f)). No twins or cracks were observed inside the grains.

IV. DISCUSSION

A. *Microstructure Characteristics*

The cast Mg-Gd-Y-Zr alloy was characterized by coarse grains and large eutectic $Mg_5(Gd,Y)$ phases at the grain boundaries. After FSP, because of the combined effect of the mechanical mixing and frictional heating generated from the FSP tool, fundamental dissolution of the $Mg_5(Gd,Y)$ phase and significant grain refinement were obtained (Figure 2). The nonsymmetric elliptical features of the SZs were present at all FSP parameters (Figure 1). The same phenomenon was observed in FSW aluminum alloys and was suggested to be caused by the asymmetric flow of plasticized materials during FSW.[16] The void at the top of the SZ in the FSP sample at 100 mm/minute might result from insufficient material flow, as reported previously in FSW aluminum alloys.[17]

The microstructure of the SZ depended on the FSP parameters. The grain size decreased with increasing travel speed. At a lower travel speed, relatively uniform microstructure was obtained throughout the SZ, whereas at a higher travel speed, a heterogeneous grain structure with evident onion rings was produced (Figures 2 and 3). The formation of these microstructures could be explained by the difference in heat input and strain rate. It is known that the heat input increased with increasing the ratio of ω/v, and the strain rate in the SZ was controlled by both the ω and v; higher ω and v produced a higher strain rate.[18,19]

At a higher travel speed, the high strain rate resulted in fine grains and a more thorough breakup of the $Mg_5(Gd,Y)$ phase, but the insufficient heat input resulted in the incomplete dissolution of the $Mg_5(Gd,Y)$ phase and insufficient material flow. Therefore, the fine grains were obtained, but the onion rings with nonuniform

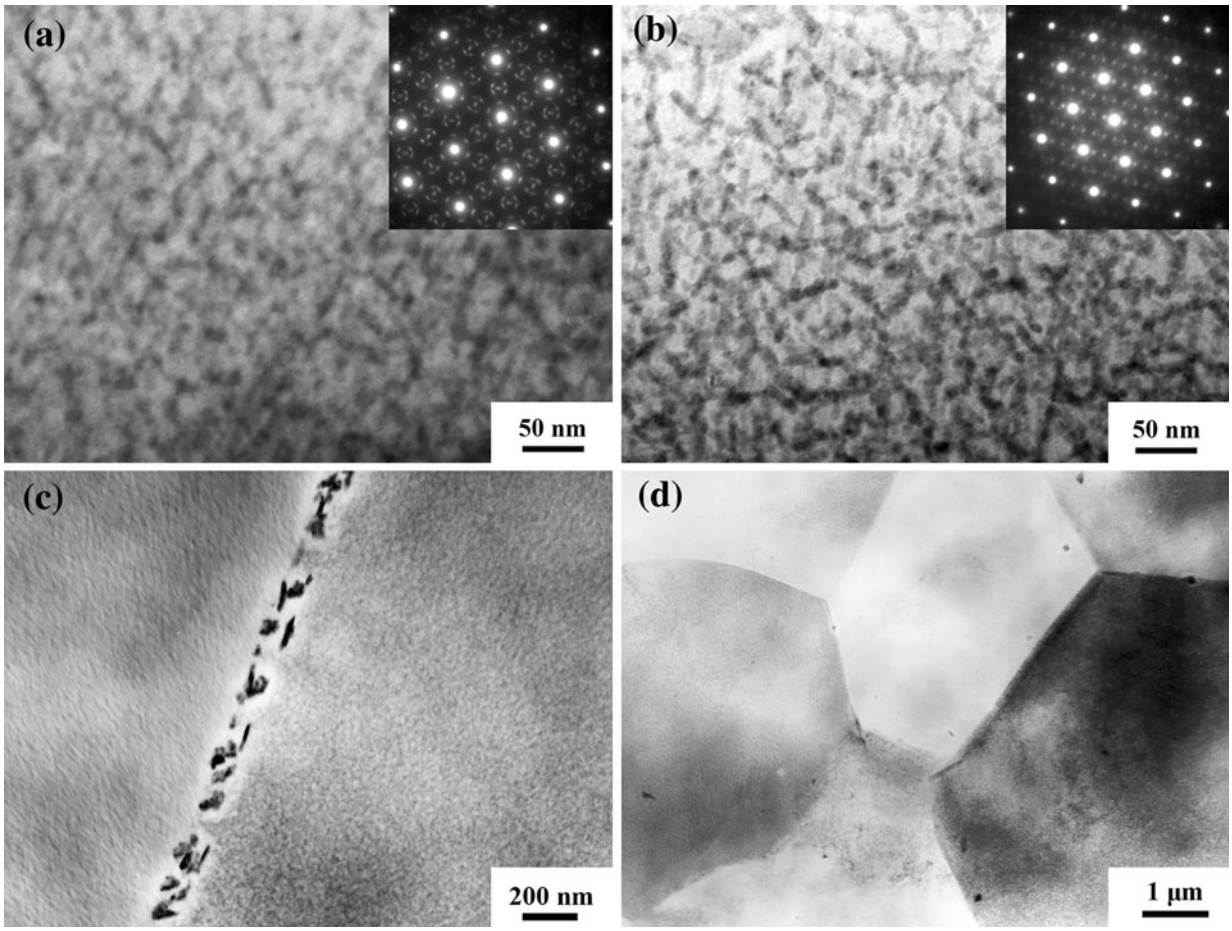

Fig. 5—TEM images of (*a*) (*c*) cast-T6 and (*b*) (*d*) FSP-T5 (800 rpm, 25 mm/min) samples.

Table I. Tensile Properties of Mg-Gd-Y-Zr Alloy in Various Conditions

Temper	YS (MPa)	UTS (MPa)	El. (pct)
Cast-T4	157 ± 6.3	224 ± 6.3	14.4 ± 2.6
FSP, 800 rpm-25 mm/min	268 ± 2.2	357 ± 0.6	24.0 ± 1.5
FSP, 800 rpm-50 mm/min	281 ± 6.6	363 ± 2.3	29.1 ± 0.4
FSP, 800 rpm-100 mm/min	214 ± 6.6	322 ± 2.1	31.0 ± 1.5

grains, bands of different solute contents, and particle bands were evident in the FSP sample at 100 mm/minute (Figures 2(d), 3(c), and 4(c)). By comparison, the FSP sample at a lower travel speed was exposed to higher temperature, and the dissolution of the $Mg_5(Gd,Y)$ particles was then enhanced; however, the higher temperature and lower strain rate resulted in the coarse grains. Therefore, a more uniform microstructure with relatively large grains was obtained in the FSP sample at 25 mm/minute (Figures 2(b), 3(a), and 4(a)). The increased width of the onion rings with increasing the travel speed was attributed to the increased v/ω value, which resulted from a geometric extrusion process.[20]

It was reported that for the cast EV31A and AZ91D magnesium alloys, the homogeneous SZ structure could be achieved at a relatively low heat input.[8,11] For a cast Mg-Al-Ca alloy containing thermally stable Al_2Ca phase, the uniform SZ with the dispersed fine Al_2Ca particles could be obtained at a low heat input parameter of 1500 rpm and 1500 mm/minute.[21] For the current Mg-Gd-Y-Zr alloy, a high heat input with the combined parameters of 800 rpm and 25 mm/minute was needed to obtain a relatively uniform microstructure. Reasons for these differences could be explained based on the second phase.

In the reported cast magnesium alloys, either the fraction of the second phase or the eutectic temperature was relatively low. For the cast EV31A and AZ91D magnesium alloys containing the dissolvable second phase with a low eutectic temperature, low values of ω and v or high values of ω and v could be applied to obtain a defect-free and uniform microstructure with dissolved particles because either the shorter duration at a higher temperature or the longer time at a lower temperature could result in the dissolution of particles.[15] For the cast Mg-Al-Ca alloy containing the

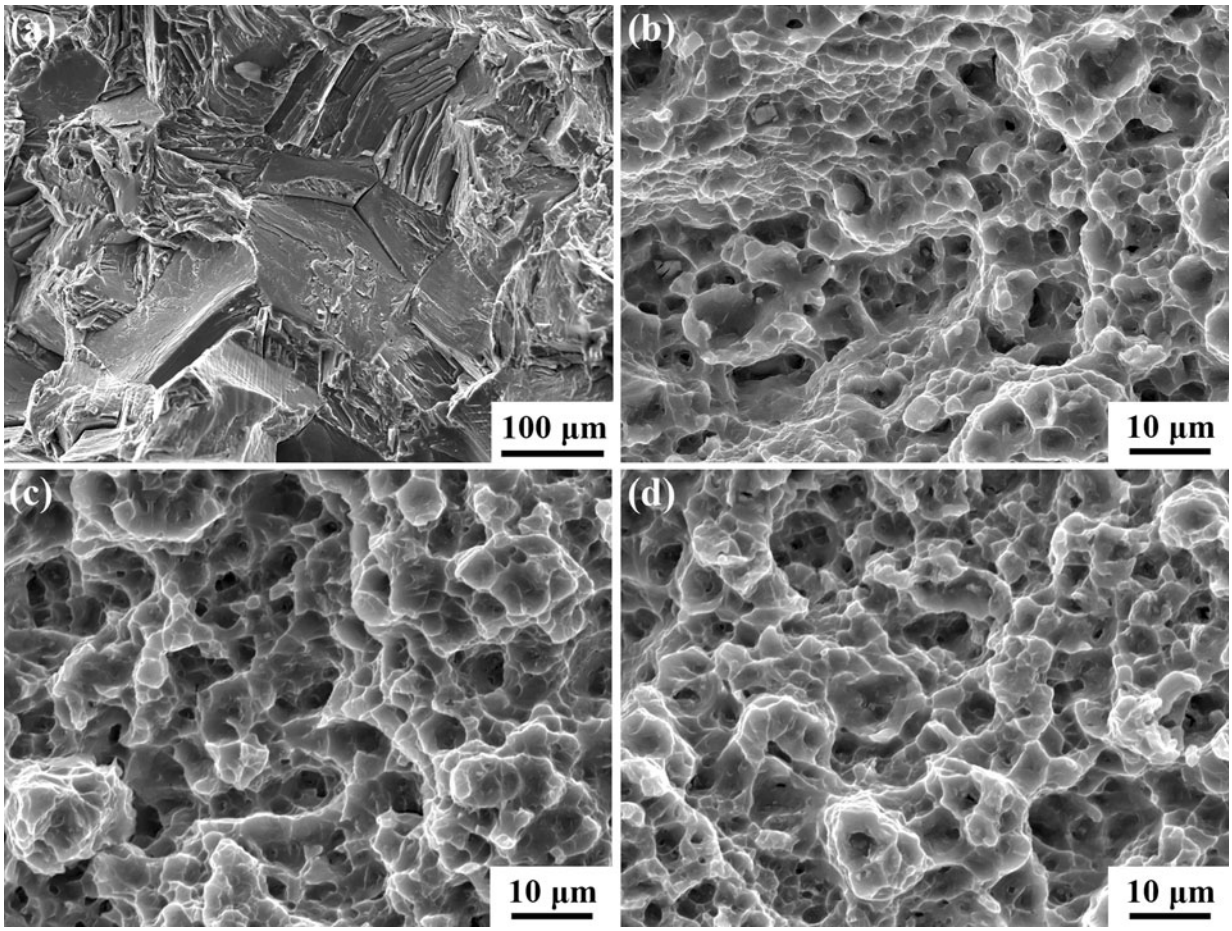

Fig. 6—Fractographs of (*a*) cast-T4 and FSP samples at different travel speeds: (*b*) 25 mm/min, (*c*) 50 mm/min, and (*d*) 100 mm/min.

Table II. Tensile Properties of FSP Sample (800 rpm, 25 mm/min) in the TD and LD

Specimen	Orientation	YS (MPa)	UTS (MPa)	El. (pct)
FSP	TD	268 ± 2.2	357 ± 0.6	24.0 ± 1.5
	LD	223 ± 3.4	323 ± 7.2	18.8 ± 0.7
FSP-T5	TD	327 ± 4.5	424 ± 8.8	6.0 ± 1.3
	LD	329 ± 4.9	418 ± 7.1	3.4 ± 0.3

indissolvable Al_2Ca particles, the strain rate played a dominant role in obtaining a uniform microstructure with refined particles. Therefore, high values of ω and v with a low heat input and high strain rate could produce a uniform microstructure with dispersed fine particles in the cast Mg-Al-Ca alloy.

In the current cast Mg-Gd-Y-Zr alloy, a high volume fraction of eutectic phase with a high eutectic temperature (~813 K [~540 °C]) was present,[22] and the diffusion rates of the Gd and Y elements in Mg are low because of their large atom radius. In this case, both a higher temperature and longer duration at high temperature are needed to dissolve the eutectics and obtain a uniform microstructure; therefore, a high heat input with low travel speed is applied. It was also observed that the grain size was relatively fine and affected weakly by the heat input; the same phenomenon was observed in a previous study.[23] This may be attributed to the solute drag of the large RE atoms and the pinning effect of the eutectic particles during FSP, which can influence strongly the recrystallization kinetics.[24,25]

The dense β' particles were observed in both the cast-T6 and FSP-T5 samples (Figure 5). The similar size and density of the β' particles in both samples indicated the similar aging response. This was coincident with the previous report that the grain size had little influence on the aging kinetics of the Mg-RE alloys.[2] However, the precipitates at the grain boundaries were different in the cast-T6 and FSP-T5 samples. The grain boundary precipitates were observed commonly in the cast-T6 sample but seldom in the FSP-T5 sample, which indicates that solute segregation at the grain boundaries still existed in the cast-T4 sample but was alleviated significantly after FSP because of the accelerated dissolution of the second phase and the diffusion of solutes promoted by the intense plastic deformation and material mixing.

B. *Mechanical Properties*

The BM exhibited low UTS of 187 MPa and YS of 178 MPa, and a low elongation of 3.2 pct because of the coarse grains and large eutectic $Mg_5(Gd,Y)$ phase.[12] After the solution treatment, the $Mg_5(Gd,Y)$ phase was

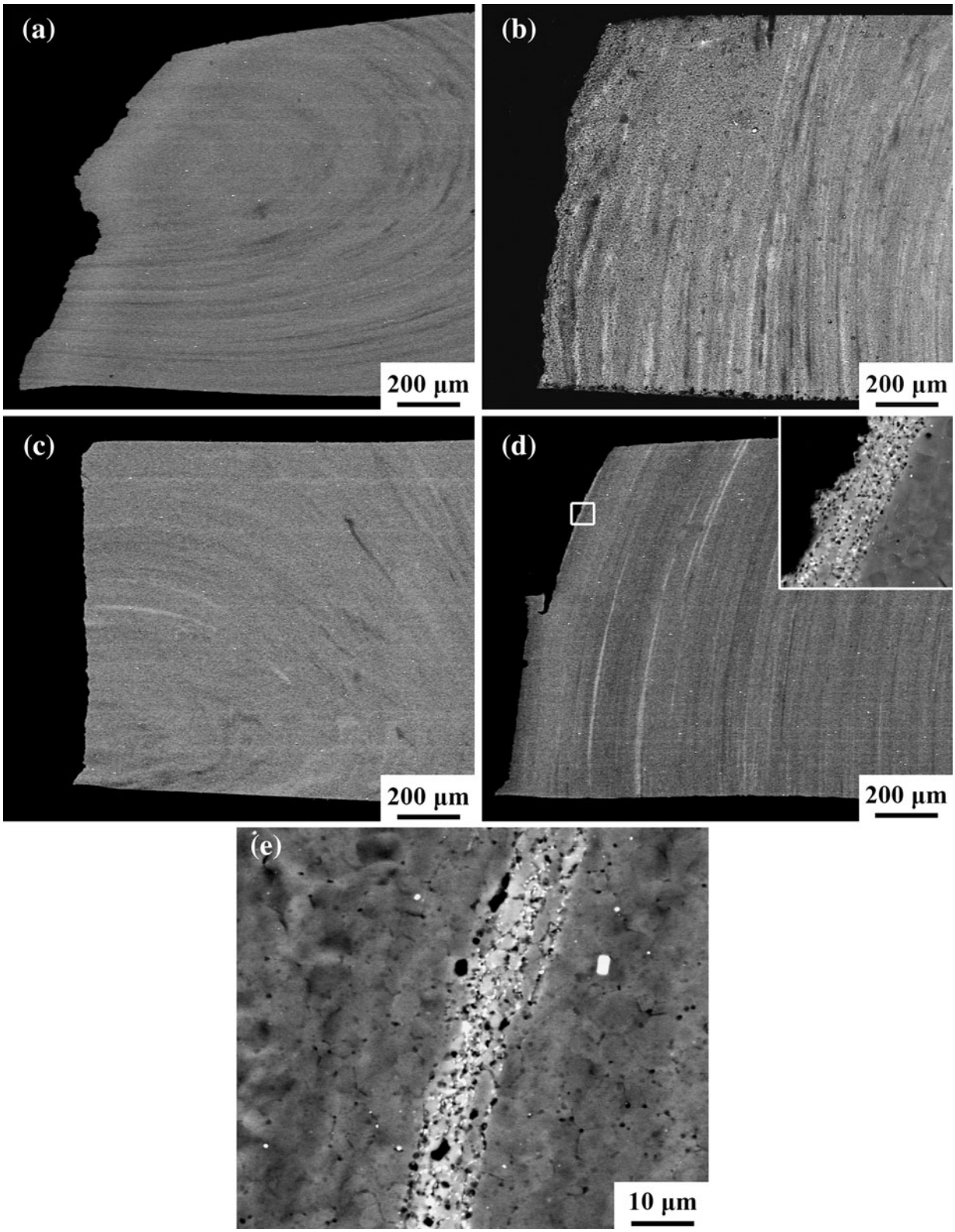

Fig. 7—Longitudinal section of failed tensile specimens for (*a*) and (*b*) FSP, and (*c*) and (*d*) FSP-T5 samples (800 rpm, 25 mm/min) in (a) and (c) TD, and (b) and (d) LD. (*e*) Particle-rich bands near the fracture tip of FSP-T5 sample in LD.

dissolved, the UTS and elongation of the cast-T4 sample were improved significantly, but the YS was reduced. The FSP samples exhibited significantly enhanced UTS, YS, and elongation compared with the cast-T4 sample (Table I). This finding is attributed to significant grain refinement and fundamental dissolution of the

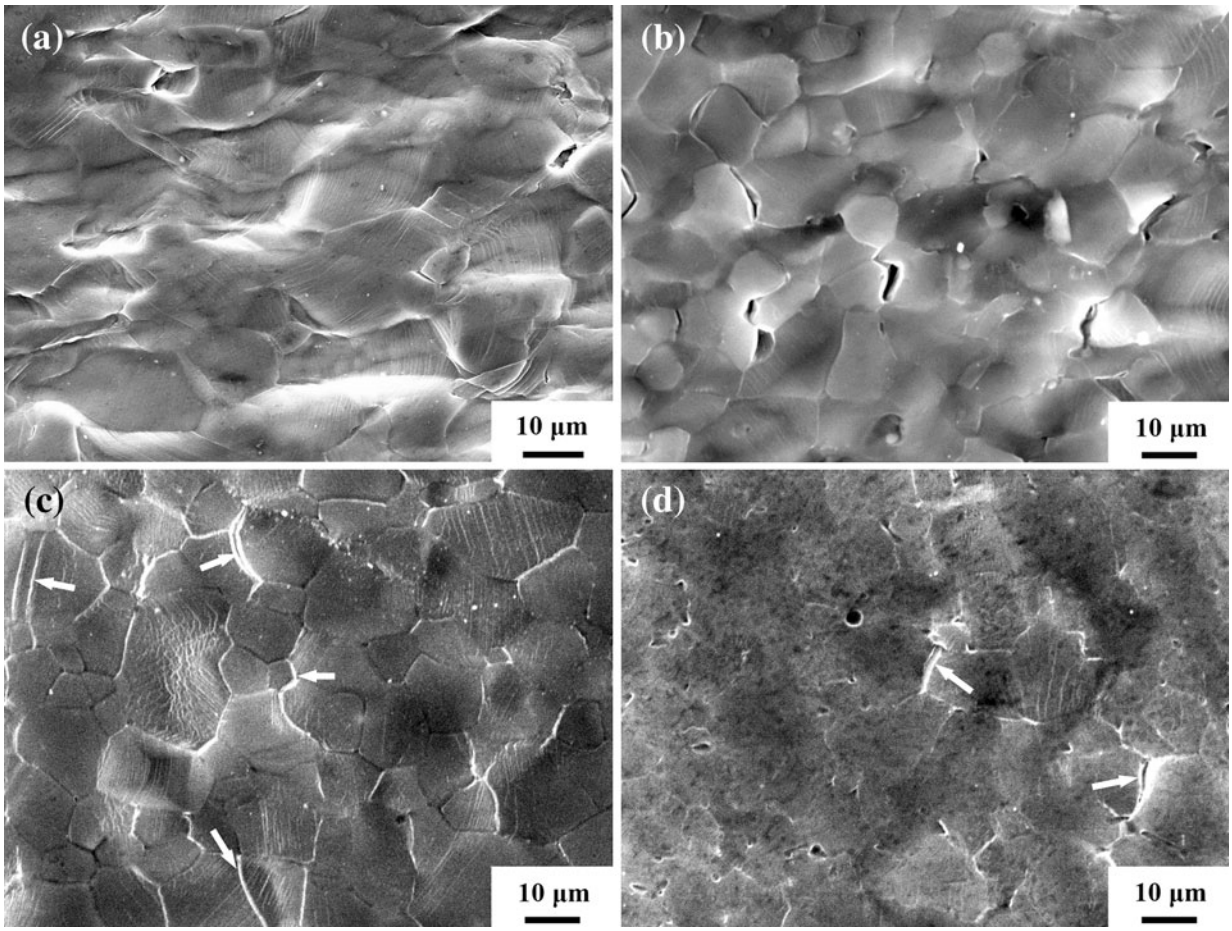

Fig. 8—Surface morphology of (*a*) and (*b*) FSP, and (*c*) and (*d*) FSP-T5 samples (800 rpm, 25 mm/min) tested in (a) and (c) TD, and (b) and (d) LD (tensile axis is horizontal).

Mg_5(Gd,Y) phase. The elongation of the FSP samples increased with increasing the travel speed. However, the UTS and YS of the FSP samples did not exhibit a monotonous increase with decreasing the grain size. It seems that the onion rings exert an influence on the variation in the strengths.

It is documented that the solid solution, precipitation, and grain refinement contribute to the strengthening of the Mg-Gd-Y-Zr alloy.[26] For the FSP samples with a fine-grained structure of nearly supersaturated solid solution, both grain refinement and solution strengthening are the main strengthening mechanisms. In all the SZs, the onion rings with alternating bands of different solute contents were observed (Figure 4). Gao *et al.*[27] found that the strengthening rate of Gd and Y atoms in the solid solution of Mg is considerably higher than that of Al and Zn. In this case, fluctuant solution strengthening would exist in the SZs: The strengthening in the black bands with low solute contents was weaker than that in the gray and white bands with medium and high solute contents. Therefore, a layered structure with varied strength was present in the SZ, and such a structure is like the laminated structure.

It was reported that for the laminates with increasing the layer thickness, the strength decreased, whereas the elongation increased.[28] The current FSP samples exhibited increased band width and reduced grain size with increasing the travel speed. Therefore, the elongation increased with the travel speed. And the variation of the tensile strength with the travel speed could be considered as the combined results of the band width and grain size. As the travel speed increased, the strengthening from the grain size increased, whereas that from the onion rings decreased. Increasing the travel speed from 25 to 50 mm/minute, the combination of the onion rings with a medium width and the fine grains with an average size of 6.1 μm contributed to the highest strength in the FSP sample with the travel speed of 50 mm/minute. At the highest travel speed of 100 mm/minute, remarkably widened onion rings reduced the strength of the FSP sample significantly, although the grain size decreased even more to 5.6 μm. Furthermore, although the particle bands existed in all the SZs, their effect on the tensile properties was small as a result of their small numbers.

C. *Tensile Properties in the TD and LD*

The anisotropy of tensile properties for the FSP sample in the TD and LD was also observed previously in magnesium alloys and was suggested to be caused by the texture variation.[29,30] In the FSP AZ31B alloy,

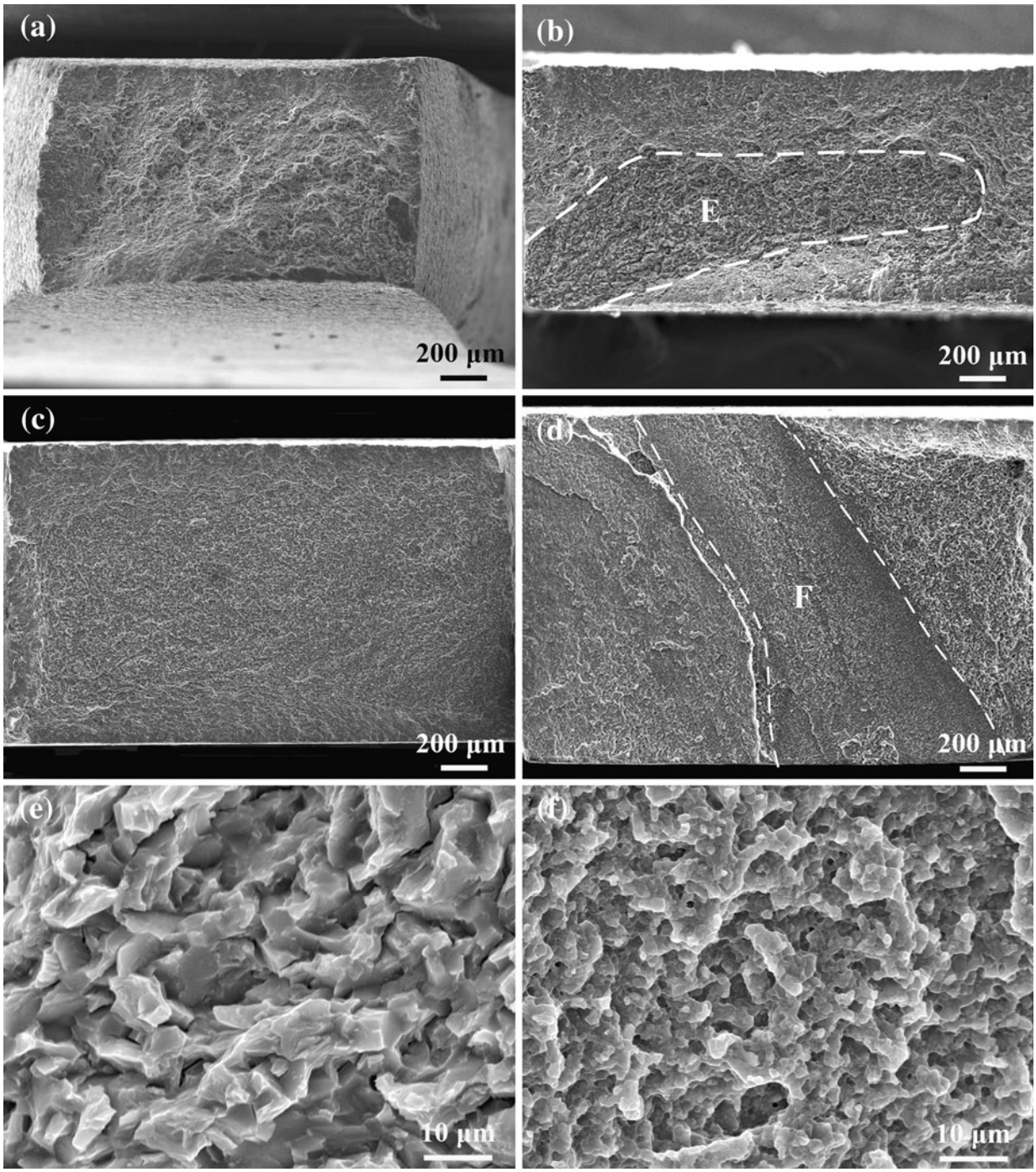

Fig. 9—Fracture surfaces of (*a*) and (*b*) FSP, and (*c*) and (*d*) FSP-T5 samples (800 rpm, 25 mm/min) tested in (a) and (c) TD, and (b) and (d) LD. (*e*) A magnified image of region E in Fig. 9(b). (*f*) A magnified image of region F in Fig. 9(d).

enhanced elongation and lower strengths were observed in the LD,[29] and these were attributed to the (0002) texture variation as a result of shear deformation during FSP. Bhargava *et al.*[30] observed that for AZ31B alloy, both the tensile strength and elongation were enhanced in the TD. They found that besides the basal plane texture, the strong $(10\bar{1}0)$ texture was also present, this strong texture caused the prismatic planes to align for easy slip during the TD test, and increased stress were then needed to activate this prismatic slip.

To evaluate the influence of texture on the TD and LD tensile properties, the Schmid factor analyses in the TD-LD and TD-ND planes for the FSP sample at 25 mm/minute were conducted using the EBSD method. The EBSD was conducted on the tensile specimens and covered the whole section of the gage region; thus the exact Schmid factors could be obtained for the tensile specimens. The distribution of the Schmid factor for the basal slip systems in the TD and LD tests is shown in Figure 13. The average Schmid factor for the TD and

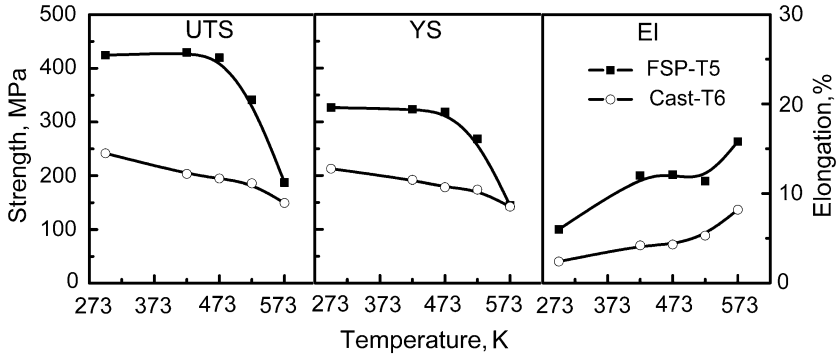

Fig. 10—Elevated temperature tensile properties of Mg-Gd-Y-Zr alloy.

LD tests was determined to 0.34 and 0.32, respectively. This finding implies that from the viewpoint of the orientation factor, the TD specimens should have lower YS than the LD ones. However, the tensile results did not follow this prediction. Thus, the texture is not the factor that resulted in the varied tensile properties in the TD and LD. The fracture surfaces in the LD test (Figures 7 and 9) indicated that the fracture behavior was related to the onion rings; thus, the low tensile properties in the LD were most likely to be caused by the onion rings.

As shown in Figure 7, the onion rings showed different morphologies in the transverse and longitudinal sections of the SZ. In the transverse section, the onion rings exhibited the feature of approximately concentric and discontinuous circles, whereas parallel and discontinuous semicircular marks were present in the longitudinal section. Therefore, the deformation conditions were different for the TD and LD tensile tests. For the TD tension, the tensile axis was almost parallel to the alternating bands, whereas for the LD tension, the tensile axis was perpendicular to these bands. It is thus proposed that for the FSP sample, the anisotropy of tensile properties could be explained by the difference in the deformation conditions.

As discussed above, the onion rings containing alternating bands were like the laminated structure. For the TD test of the FSP sample, these bands were roughly on the isostrain orientation,[31,32] and the strength contribution of these bands followed the rule of mixture. It is known that the layer thickness and the constituent materials could affect the deformation behavior of the laminates. The thin layers and the low mechanical dissimilarity between the constituent materials could generate uniform deformation and enhance the fracture elongation.[33] In the TD test, the deformation surface and fractograph of the FSP sample exhibited the uniform deformation (Figures 8(a) and 9(a)). This might result from the narrow bands with a width of approximately 50 μm and the low mechanical dissimilarity between these bands, as they differed in the solute contents inside the grains. Therefore, enhanced tensile elongation was obtained in the TD test for the FSP sample.

For the LD test of the FSP sample, these bands were perpendicular to the tensile axis. The tensile strength was the minimum strength of these bands, *i.e.*, the black bands. Therefore, lower tensile strength was observed in the LD than in the TD. As a result of localized deformation in the soft black bands, the stress concentration was generated in the interfaces of the black band/matrix or the black band/white band, causing early failure of the LD specimen. This is supported by the deformation and fracture surfaces. On the longitudinal section of the failed specimen, the fracture path followed the black bands well, indicating the localized deformation at the black bands. The lack of extensive slip lines (Figure 8(b)) and the unevenly distributed cracks on the deformed surface were indicative of the nonuniform deformation. The brittle rupture part on the fracture surface also indicated this nonuniform deformation, and its termination in the middle section of the tensile specimen (Figure 9(b)) would be attributed to the discontinuity of these bands, as shown in Figure 7(b). Therefore, lower elongation was observed in the LD test.

For the FSP-T5 sample, the precipitation of densely distributed, nanosized β' particles (Figure 5(b)) significantly enhanced the strength and reduced elongation compared with the FSP sample. In this case, precipitation strengthening was the main strengthening mechanism in the FSP-T5 sample. However, different from that for the FSP sample, the strength anisotropy in the TD and LD for the FSP-T5 sample disappeared, which is attributed to the similar precipitation strengthening effect. For the Mg-RE alloys, a previous study indicated that the increase of supersaturation could accelerate the aging kinetics.[2] For the black bands with low solute content, the age-hardening response was slower than that for gray and white bands with medium and high solute contents. Therefore, the size or density of the precipitates might vary between these bands after aging for 13 h. This hypothesis was confirmed by Anyanwu *et al.*,[34] who studied the aging characteristics of Mg-Gd-Y-Zr with different solute contents. They observed that the precipitates decreased in number and became coarser as the Gd content decreased, and the peak hardness gradually decreased with increasing the Y/Gd ratio when aged at 498 K (225 °C).[34]

According to previous studies on the Mg-Gd-Y-Zr alloy with the similar solute contents as the present bands, aging at 498 K (225 °C) for 13 h could reach the

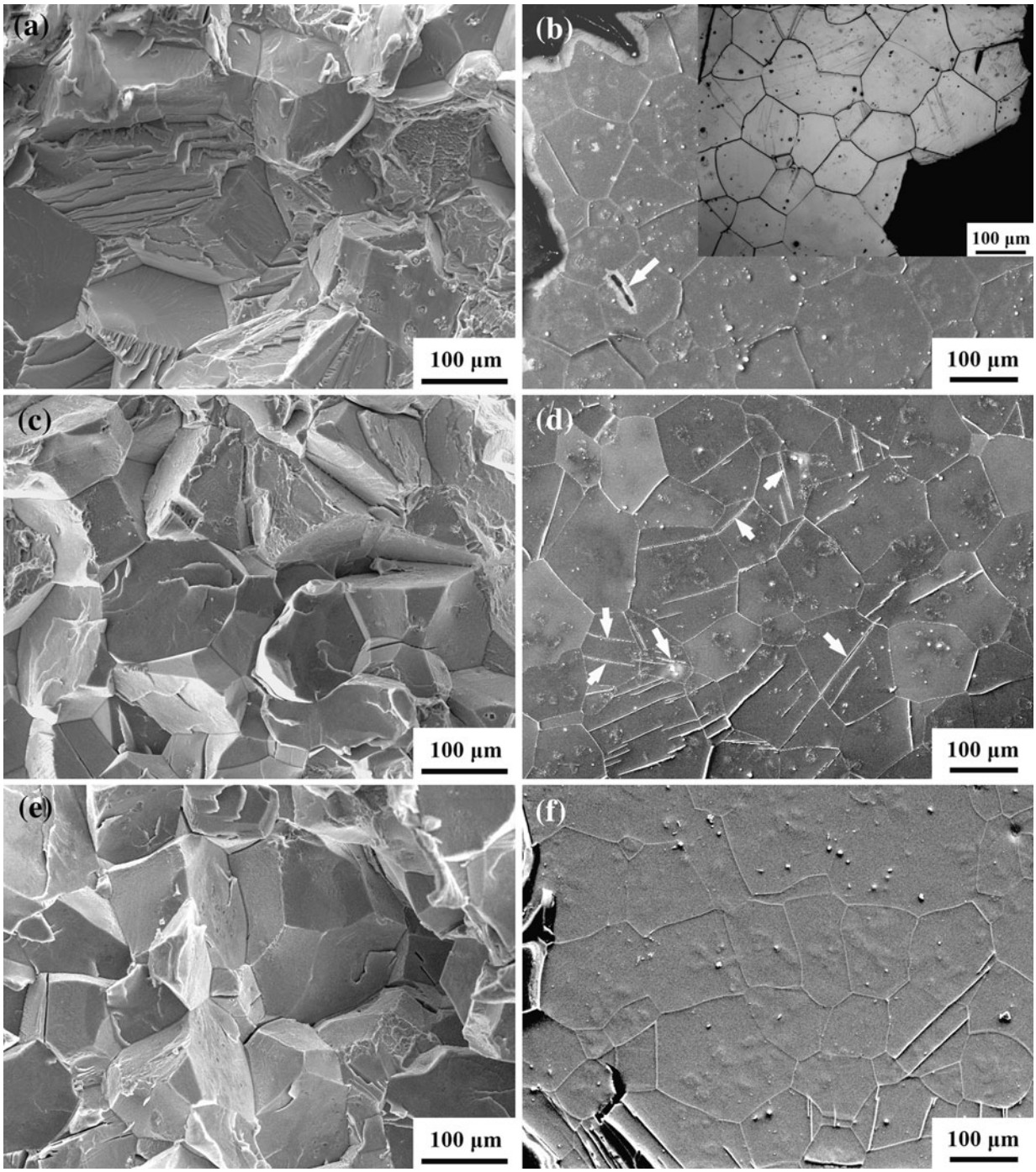

Fig. 11—SEM images of fracture surfaces ((*a*), (*c*), and (*e*)) and longitudinal sections ((*b*), (*d*), and (*f*)) near fracture tip of cast-T6 sample at (a) and (b) room temperature, (c) and (d) 523 K (250 °C), and (e) and (f) 573 K (300 °C).

peak hardness.[26,34] Thus, the bands with solute content difference in the FSP-T5 sample were all on the peak aging condition. The Y/Gd mol ratio in the black, gray and white bands was 0.55, 0.45, and 0.47, respectively, and the hardness in these bands should be almost the same according to the study of Anyanwu *et al.*[34] In this case, despite the differences in the precipitates, the precipitation strengthening effect in various bands had little difference. So the effect of solute content differences on the strengths in the LD test was not as evident in the FSP-T5 sample as in the FSP sample, and the strengths in the TD and LD were almost the same.

Although the bands with different solute contents had little influence on the tensile strength anisotropy of the FSP-T5 sample, the small amount of particle bands did affect the tensile elongation. The fracture surface of the TD specimen showed the uniform fracture mode (Figure 9(c)) as a result of uniform deformation. For the LD tension, the breakup of the particle bands (Figure 7(d)) led to the early failure of the specimen, and a low

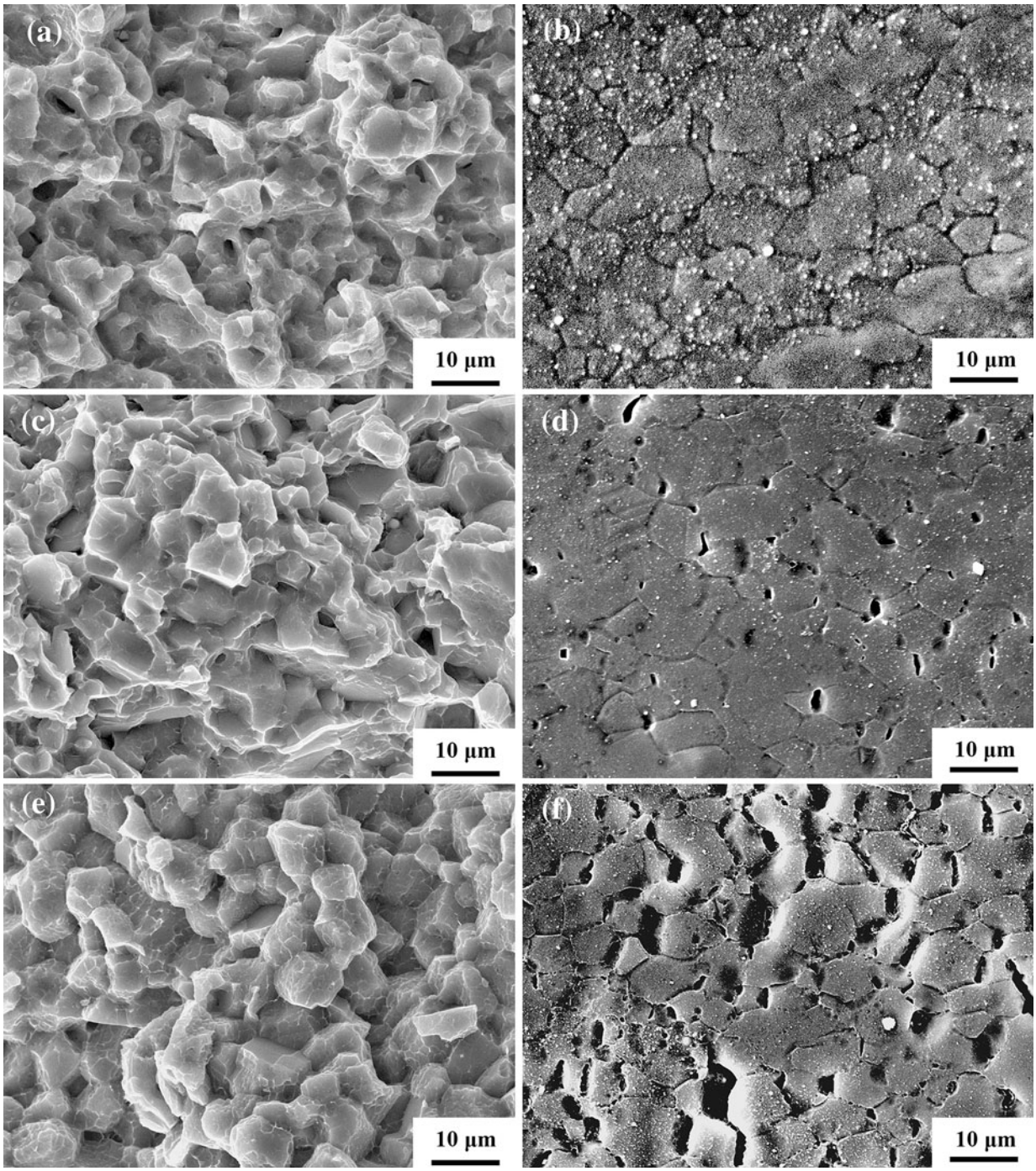

Fig. 12—SEM images of fracture surfaces ((*a*), (*c*), and (*e*)) and longitudinal sections ((*b*), (*d*), and (*f*)) near fracture tip of FSP-T5 sample at (a) and (b) room temperature, (c) and (d) 523 K (250 °C), (e) and (f) 573 K (250 °C).

elongation was obtained. This result was justified by the deformation and fracture surfaces. The microvoids on the LD deformation surface (Figure 8(d)) and the extensive microvoids located at these particles in Figures 7(d) and (e) were indicative of the local stress concentration at the particles, these voids would interlink in the particle bands and cause early failure of the FSP-T5 sample. The region with small and flat dimples on the LD fracture surface (Figure 9(d)) was also indicative of failure at the particle bands with dense and fine particles. It is observed that the fracture location of the LD tensile specimens shifted from the black bands in the FSP condition to the particle-rich band in the FSP-T5 condition. The reason for this was the sensitivity of the high-strength FSP-T5 samples to local stress concentration generated in the particle bands perpendicular to the tensile axis in the LD test.

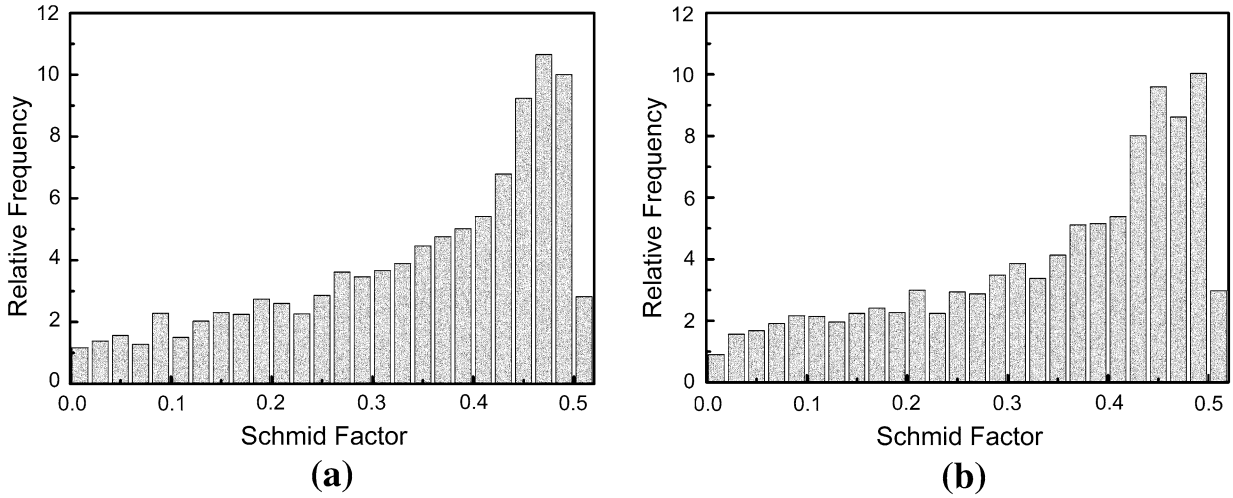

Fig. 13—Schmid factor distributions of the (0001) <11-20> slip systems in (*a*) TD and (*b*) LD.

D. *High-Temperature Tensile Properties*

The FSP-T5 sample exhibited superior strength and enhanced elongation compared with the cast-T6 sample. This was attributed to the fine grains and thermally stable β' phase as identified in Figure 5. The effective pinning effect of β' precipitates on the basal slip resulted in high strength even at 473 K (200 °C). At above 498 K (225 °C), rapid deterioration of strength occurred for the FSP-T5 sample because of the coarsening of the precipitates and the reduced blocking effect of the β' precipitates to the activated nonbasal gliding. It is noted that because of the coarse grains, the strength deterioration rate of the cast-T6 sample was lower than that of the FSP-T5 sample.

As observed from all the fractographs, no obvious deformation on the cleavage planes or the small facets was observed, so the elongation of both the as-cast and FSP samples was relatively low even at high temperatures. Note that the intergranular rupture was commonly observed at all temperatures in the cast-T6 sample but seldom observed in the FSP-T5 sample even at 473 K (200 °C). This intergranular fracture in the cast-T6 sample could be caused by the presence of grain-boundary precipitates (Figure 5(b)).

The deformation mechanisms of the cast-T6 and FSP-T5 samples were different. Twins were observed in the deformed cast-T6 sample at all testing temperatures. The occurrence of twins even at high temperatures was probably a result of the low ductility caused by the coarse grains and dense precipitates, and even the activation of nonbasal slip could not accommodate the deformation. The extensive cracks occurred and propagated along the boundaries between the twins and the matrix at all temperatures (Figure 11). This failure mechanism was commonly observed in deformed coarse-grained magnesium alloys, and it was suggestive of the local stress concentration generated by twins.[35] So the dominant deformation mechanism of the cast-T6 sample was twin deformation even at high temperatures. No twins were observed at all testing temperatures in the FSP-T5 sample. The grain boundary voids and their interlinkage were observed as the temperature increased. Therefore, the deformation mechanism of the FSP-T5 sample was dislocation slip accompanied by void growth.

V. CONCLUSIONS

1. FSP resulted in significant grain refinement and fundamental dissolution of the eutectic $Mg_5(Gd,Y)$ phase in the Mg-Gd-Y-Zr casting. At the investigated travel speeds of 25 to 100 mm/minute, the onion rings with bands of different solute contents were observed. As the travel speed increased, the grain size decreased and the banded structure became evident.
2. Compared with the cast BM, the FSP samples exhibited remarkably enhanced tensile properties. As the travel speed increased from 25 to 100 mm/minute, the elongation of the FSP sample increased; however, the highest strengths were obtained at a medium travel speed of 50 mm/minute. Furthermore, the FSP samples exhibited a tensile anisotropy; both the strengths and elongation were higher in the TD than in the LD.
3. After post-FSP aging, the strengths of the FSP samples were significantly increased and the elongation was reduced. The strengths in the TD and LD were almost the same, whereas lower elongation was observed in the LD.
4. The FSP samples showed enhanced tensile properties at high temperatures compared with the cast BM. High yield strength of above 250 MPa was kept even at 523 K (250 °C).

ACKNOWLEDGMENTS

This work was supported by the National Natural Science Foundation of China under Grant No.

50901075, the National Basic Research Program of China under Grant No. 2011CB606301, and the National Outstanding Young Scientist Foundation of China under Grant No. 50525103.

REFERENCES

1. B.L. Mordike and T. Ebert: *Mater. Sci. Eng. A*, 2002, vol. 302, pp. 37–45.
2. L.L. Rokhlin: *Magnesium Alloys Containing Rare Earth Metals: Structure and properties*, Taylor and Francis, London, UK, 2003.
3. J.P. Li, Z. Yang, and T. Liu: *Scripta Mater.*, 2007, vol. 56, pp. 137–40.
4. R.G. Li, J.F. Nie, G.J. Huang, Y.C. Xin, and Q. Liu: *Scripta Mater.*, 2011, vol. 64, pp. 950–53.
5. R.S. Mishra and Z.Y. Ma: *Mater. Sci. Eng. R*, 2005, vol. 50, pp. 1–78.
6. A.H. Feng, B.L. Xiao, Z.Y. Ma, and R.S. Chen: *Metall. Mater. Trans. A*, 2009, vol. 40A, pp. 2447–56.
7. M. Santella, A. Frederick, C. Degen, and T.Y. Pan: *JOM*, 2006, vol. 58, pp. 56–61.
8. A.H. Feng and Z.Y. Ma: *Scripta Mater.*, 2007, vol. 56, pp. 397–400.
9. D.R. Ni, D. Wang, A.H. Feng, G. Yao, and Z.Y. Ma: *Scripta Mater.*, 2009, vol. 61, pp. 568–71.
10. M. Tsujikawa, S.W. Chung, and M. Tanaka: *Mater. Trans.*, 2005, vol. 46, pp. 3081–84.
11. T.A. Freeney and R.S. Mishra: *Metall. Mater. Trans. A*, 2010, vol. 41A, pp. 73–84.
12. B.L. Xiao, Q. Yang, J. Yang, W.G. Wang, G.M. Xie, and Z.Y. Ma: *J. Alloys Compd.*, 2011, vol. 509, pp. 2879–84.
13. M.W. Mahoney, C.G. Rhodes, J.G. Flintoff, W.H. Bingel, and R.A. Spurling: *Metall. Mater. Trans. A*, 1998, vol. 29A, pp. 1955–64.
14. M.A. Sutton, B. Yang, A.P. Reynolds, and R. Taylor: *Mater. Sci. Eng. A*, 2002, vol. 323A, pp. 160–66.
15. Z.Y. Ma, A.L. Pilchak, and M.C. Juhas: *Scripta Mater.*, 2008, vol. 58, pp. 361–66.
16. T.U. Seidel and A.P. Reynolds: *Metall. Mater. Trans. A*, 2001, vol. 32A, pp. 2879–84.
17. Z.W. Chen, T. Pasang, and Y. Qi: *Mater. Sci. Eng. A*, 2008, vol. 474A, pp. 312–16.
18. C.I. Chang, C.J. Lee, and J.C. Huang: *Scripta Mater.*, 2004, vol. 51, pp. 509–14.
19. K.A.A. Hassan, P.B. Prangnell, A.F. Norman, D.A. Price, and S.W. Williams: *Sci. Technol. Weld. Join.*, 2003, vol. 8, pp. 257–68.
20. K.N. Krishnan: *Mater. Sci. Eng. A*, 2002, vol. 327A, pp. 246–51.
21. D. Zhang, M. Suzuki, and K. Maruyama: *Scripta Mater.*, 2005, vol. 52, pp. 899–903.
22. Y. Gao, Q.D. Wang, J.H. Gu, Y. Zhao, and Y. Tong: *Mater. Sci. Eng. A*, 2007, vol. 459A, pp. 117–23.
23. T.A. Freeney, R.S. Mishra, G.J. Grant, and R. Verma: *Friction Stir Welding and Processing IV*, TMS, Warrendale, PA, 2007.
24. K. Lücke and K. Deter: *Acta Metall.*, 1957, vol. 5, pp. 628–37.
25. J. Bohlen, M.R. Nürnberg, J.W. Senn, D. Letzig, and S.R. Agnew: *Acta Mater.*, 2007, vol. 55, pp. 2101–12.
26. S.M. He, X.Q. Zeng, L.M. Peng, X. Gao, J.F. Nie, and W.J. Ding: *J. Alloys Compd.*, 2007, vol. 427, pp. 316–23.
27. L. Gao, R.S. Chen, and E.H. Han: *J. Alloys Compd.*, 2009, vol. 481, pp. 379–84.
28. K.S. Ravichandran, S.S. Sahay, and J.G. Byrne: *Scripta Mater.*, 1996, vol. 35, pp. 1135–40.
29. W. Woo, H. Choo, D.W. Brown, P.K. Liaw, and Z. Feng: *Scripta Mater.*, 2006, vol. 54, pp. 1859–64.
30. G. Bhargava, W. Yuan, S.S. Webb, and R.S. Mishra: *Metall. Mater. Trans. A.*, 2010, vol. 41A, pp. 13–17.
31. J. Wang, E.M. Taleff, and D. Kovar: *Acta Mater.*, 2004, vol. 52, pp. 4685–93.
32. J.D. French, J.H. Zhao, M.P. Harmer, H.M. Chan, and G.A. Miller: *J. Am. Ceram. Soc.*, 1994, vol. 77, pp. 2857–65.
33. J. Inoue, S. Nambu, Y. Ishimoto, and T. Koseki: *Scripta Mater.*, 2008, vol. 59, pp. 1055–58.
34. I.A. Anyanwu, S. Kamado, and Y. Kojima: *Mater. Trans.*, 2001, vol. 42, pp. 1206–11.
35. H. Somekawa, A. Singh, and T. Mukai: *Phil. Mag. Lett.*, 2009, vol. 89, pp. 2–10.